Proceedings of the 17th World Congress
The International Federation of Automatic Control
Seoul, Korea, July 6-11, 2008

Backstepping Control of a High-Speed Linear Axis Driven by Pneumatic Muscles

D. Schindele * **H. Aschemann** *

* *Chair of Mechatronics, University of Rostock, D-18059 Rostock, Germany*
(e-mail: {dominik.schindele, harald.aschemann}@uni-rostock.de)

Abstract: This paper presents a backstepping control scheme for a new linear axis. Its guided carriage is driven by a nonlinear mechanism consisting of a rocker with a pair of pneumatic muscle actuators arranged at both sides. This innovative drive concept allows for an increased workspace as well as higher carriage velocities as compared to a direct actuation. Modelling leads to a system of nonlinear differential equations including polynomial approximations of the volume characteristic as well as the force characteristic of the pneumatic muscles. The proposed control has a cascade structure: The internal pressure of each pneumatic muscle is controlled by a fast underlying control loop, whereas in an outer control loop the carriage position and the mean internal pressure of the muscles are controlled. Remaining model uncertainties as well as nonlinear friction can be counteracted either by an observer-based disturbance compensation or an adaptive control strategy. Experimental results from an implementation on a test rig show a high control performance. *Copyright©2008 IFAC*

Keywords: Mechatronics, pneumatic muscles, backstepping, nonlinear systems

1. INTRODUCTION

As shown in earlier work (Schindele and Aschemann [2007], Aschemann and Schindele [2007], Aschemann et al. [2006]) pneumatic muscles in combination with sophisticated nonlinear control can be used in motion control applications where precise tracking control of desired trajectories is required. Due to this fact, current research at the University of Rostock focuses on the use of pneumatic muscles as low-cost actuators in robotics. Pneumatic muscles are tension actuators consisting of a fiber-reinforced vulcanised rubber tubing with connection flanges at both ends. Because of a special fiber arrangement, the pneumatical muscle contracts with increasing internal pressure, which can be used for actuation purposes. Pneumatic muscles offer major advantages in comparison to classical pneumatic cylinders. They have significantly less weight, there are no stick-slip effects, the muscles are insensitive to dirty working environment and they have a larger maximum force. The nonlinear characteristics of the muscle, however, demand for nonlinear control, e.g. NMPC in earlier research, see Schindele and Aschemann [2007]. In Aschemann and Schindele [2007], a nonlinear control scheme for a one-degree-of-freedom linear axis directly driven by pneumatic muscles was presented, which allows for horizontal movements. To increase both the available workspace and the maximum velocity of the carriage, a new nonlinear drive mechanism is employed as depicted in fig. 1. Here, two guideways with roller bearing units allow for rectilinear movements of the carriage with relatively small friction forces. The carriage is driven by a rocker. A bearing unit at the head of the rocker allows for both rotational and translational relative motion and transmits the drive force to the carriage. The rocker is actuated by a pair of pneumatic muscles in an antagonistic arrangement. The mounting points of the pneumatic muscles at the rocker have be defined so as to gain a reasonable trade-off between increase in maximum velocity and reduction of the achievable drive force. The mass flow rate of compressed

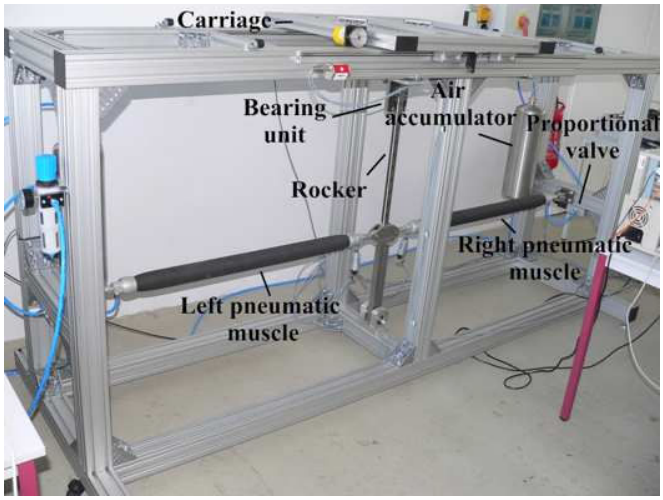

Fig. 1. High-speed linear axis

air into respectively out of each pneumatic muscle is controlled by means of a separate proportional valve. The incoming air is available at a maximum pressure of 7 *bar*, whereas the outlet air is discharged at atmospheric pressure, i.e. 1 *bar*. Pressure declines in the case of large mass flow rates are avoided by using an air accumulator for each muscle.
The paper is structured as follows: first, the modelling of the mechatronic system is addressed. For the nonlinear characteristics of the pneumatic muscle, i.e. the muscle volume and the muscle force, polynomial descriptions are used in terms of contraction length and internal muscle pressure. Second, a nonlinear cascade control scheme for the linear axis is proposed. Backstepping controllers have been designed for the inner control loops for the internal muscle pressures as well as for the outer control loop, where the carriage position and the mean pressure of the both pneumatic muscles are the controlled

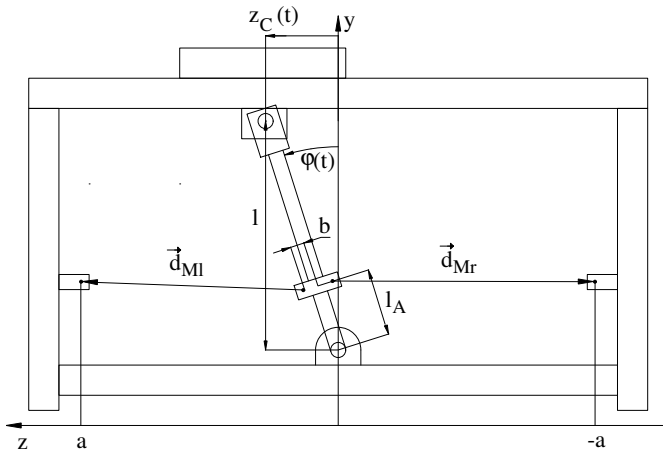

Fig. 2. Kinematical structure of the high-speed linear axis

variables. The reference pressures for the inner pressure control loops are provided by the outer control loop. A disturbance force resulting from remaining modelling errors w.r.t. the force characteristic of the pneumatic muscles as well as the friction characteristic of the carriage is compensated either by an adaptive estimation scheme or by a nonlinear reduced-order disturbance observer. By this, desired trajectories for both carriage position and mean pressure can be tracked with high accuracy as shown by experimental results from an implementation at a test rig.

2. MODELLING OF THE MECHATRONIC SYSTEM

As for modelling, the mechatronic system under consideration is divided in a mechanical and a pneumatic subsystem, which are coupled by the drive torque resulting from the tension forces of the pair of pneumatic muscles. In contrast to the model of Carbonell et al. [2001], the dynamics of the pneumatic subsystem is taken into consideration as well.

2.1 Modelling of the mechanical subsystem

The chosen mechanical model for the high-speed linear axis consists of the following three elements (fig. 2): a rigid body for the rocker as actuated link (mass m_R, reduced mass moment of inertia w.r.t. the rocker joint J_R, distance s_R to the centre of gravity C_R, varying length of the link l_R), a single lumped mass for the lateral connecting rods (mass m_A, centre of gravity distance l_A to the rocker joint) and a lumped mass for the carriage (mass m_C).
The inertial yz-coordinate system is chosen in the base joint of the rocker. The mounting points of the pneumatic muscles at the rocker are characterised by the distance l_A in longitudinal direction and the perpendicular distance b of the lateral connecting rods as shown in fig. 2. The motion of the high-speed axis is completely described by the generalised coordinate $\varphi(t)$, which denotes the inclination of the rocker w.r.t. the plumb line. The carriage position is related to the rocker angle by the horizontal component $z_C(t) = l \cdot \tan\varphi(t)$, where l denotes the length between the mounts at the head and the bottom of the rocker at carriage position $z_C = 0$.
The equation of motion directly follows from Lagrange's equations in form of a second order differential equation

$$J(\varphi)\ddot{\varphi} + k(\varphi,\dot{\varphi}) = \tau - \tau_U \ , \qquad (1)$$

with the resulting mass moment of inertia $J(\varphi) = m_C \cdot l^2 \cdot (1+\tan\varphi^2)^2 + J_R + m_A \cdot l_A^2$ and the term $k(\varphi,\dot{\varphi}) = 2 \cdot m_C \cdot l^2 \cdot (1+\tan\varphi^2)^2 \cdot \tan\varphi \cdot \dot{\varphi}^2 - (m_R/2 \cdot l + m_A \cdot l_A) \cdot g \cdot \sin\varphi$, which takes into account the centrifugal as well as the gravity forces. The drive torque τ resulting from the muscle forces F_{Mi}, $i = \{l,r\}$ can be stated as

$$\tau = \vec{e}_x \cdot (F_{Mr} \cdot \vec{r}_{Fr} \times \vec{e}_{Mr} + F_{Ml} \cdot \vec{r}_{Fl} \times \vec{e}_{Ml}) \ , \qquad (2)$$

with the unity vector $\vec{e}_x = [1,0,0]^T$ in x-direction and the unity vectors $\vec{e}_{Mi} = \vec{d}_{Mi} / d_{Mi}$ in direction of the pneumatic muscle forces. The position vectors $\vec{r}_{Fi}$ describe the connecting points, where the muscle forces act on the rocker.
All remaining model uncertainties are taken into account by the disturbance torque τ_U. On the one hand, these uncertainties stem from approximation errors concerning the static muscle force characteristics and non-modelled viscoelastic effects of the vulcanised rubber material. On the other hand, time-varying damping and friction acting on the carriage as well as on the rocker depend in a complex manner on lots of influence factors and cannot be accurately represented by a simple friction model.

2.2 Modelling of the pneumatic subsystem

A mass flow $\dot{m}_{Mi}$, $i = \{l,r\}$ into the pneumatic muscle leads to an increase in internal pressure p_{Mi}, and a contraction $\Delta\ell_{Mi}$ of the muscle in longitudinal direction due to specially arranged fibers. The maximum contraction length $\Delta\ell_{M,max}$ is given by 25% of the uncontracted length. This contraction effect can be exploited to generate forces. The force F_{Mi} and the volume V_{Mi} of a pneumatic muscle depend nonlinear on the according internal pressure p_{Mi} and the contraction length $\Delta\ell_{Mi}$. The definition of the contraction length can be derived from fig. 2. Given the length of the uncontracted muscle ℓ_M, the contraction length of a pneumatic muscle can be calculated with the distance $d_{Mi} = |\vec{d}_{Mi}|$ between both connecting points of each muscle $i = \{l,r\}$. Simple geometrical considerations lead to the length of the left respectively right pneumatic muscle

$$d_{Mi} = \sqrt{d_{Miy}^2 + d_{Miz}^2} \ , \qquad (3)$$

with $d_{Miy} = -\ell_A \cdot \cos\varphi \pm b \cdot \sin\varphi + \ell_A$ and $d_{Miz} = -\ell_A \cdot \sin\varphi \mp b \cdot \cos\varphi \pm a$. As a result, the contraction lengths for both pneumatic muscles are related to the rocker angle

$$\Delta\ell_{Mi} = \ell_M - d_{Mi}(\varphi) \ . \qquad (4)$$

The dynamics of the internal muscle pressure follows directly from a mass flow balance in combination with the energy equation for the compressed air in the muscle. As the internal muscle pressure is limited by a maximum value of $p_{Mi,max} = 7\ bar$, the ideal gas equation represents an accurate description of the thermodynamic behaviour. The thermodynamic process is modelled as a polytropic change of state with $n = 1.26$ as identified polytropic exponent. The identified volume characteristic (fig. 3) of the pneumatic muscle can be described by a polynomial function of both contraction length $\Delta\ell_{Mi}$ and the muscle pressure p_{Mi}

$$V_{Mi}(\Delta\ell_{Mi}, p_{Mi}) = \sum_{j=0}^{3} a_j \cdot \Delta\ell_{Mi}^j \cdot \sum_{k=0}^{1} b_k \cdot p_{Mi}^k . \qquad (5)$$

The resulting state equation for the internal muscle pressure in the muscle i is given by

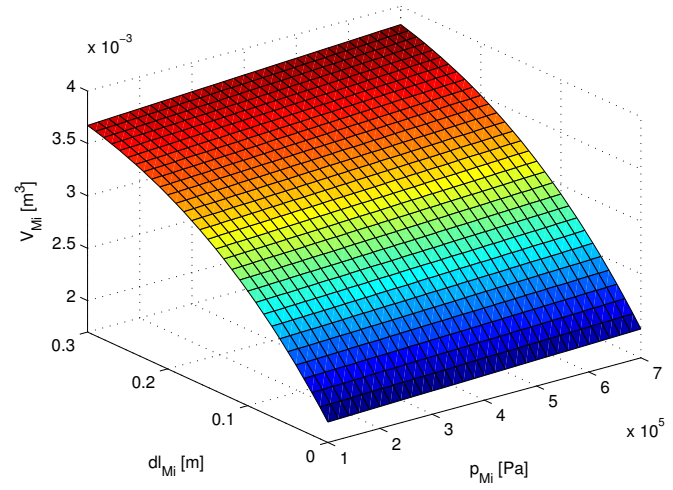

Fig. 3. Identified volume characteristic of the pneumatic muscle

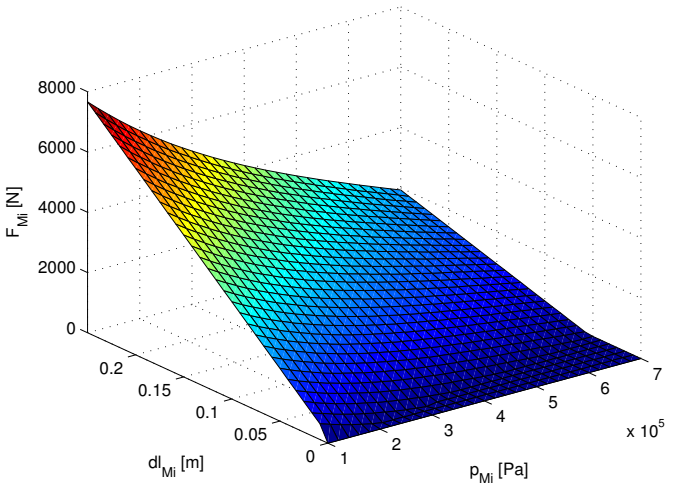

Fig. 4. Identified force characteristic of the pneumatic muscle

$$\dot{p}_{Mi} = \frac{n}{V_{Mi} + n \cdot \frac{\partial V_{Mi}}{\partial p_{Mi}} \cdot p_{Mi}} \Big[R_L \cdot T_{Mi} \cdot \dot{m}_{Mi} - \frac{\partial V_{Mi}}{\partial \Delta \ell_{Mi}} \cdot \frac{\partial \Delta \ell_{Mi}}{\partial \varphi} \cdot p_{Mi} \cdot \dot{\varphi} \Big] , \tag{6}$$

where R_L denotes the gas constant of air. The internal temperature T_{Mi} can be approximated with good accuracy by the constant temperature T_0 of the ambiance, see Göttert [2004]. In this way, temperature measurements can be avoided, and the implementational effort is significantly reduced.
The force characteristic $F_{Mi}(p_{Mi}, \Delta \ell_{Mi})$ of a pneumatic muscle states the resulting tension force for given internal pressure p_{Mi} as well as given contraction length $\Delta \ell_{Mi}$ and represents the connection of the mechanical and the pneumatic system part. The nonlinear force characteristic (fig. 4) has been identified by static measurements and, then, approximated by the following polynomial description

$$\begin{aligned} F_{Mi}(p_{Mi}, \Delta \ell_{Mi}) &= \sum_{m=0}^{3} (a_m \cdot \Delta \ell_{Mi}^m) \cdot p_{Mi} - \sum_{n=0}^{4} (b_n \cdot \Delta \ell_{Mi}^n) \\ &= \bar{F}_{Mi}(\Delta \ell_{Mi}) \cdot p_{Mi} - f_{Mi}(\Delta \ell_{Mi}) \ . \end{aligned} \tag{7}$$

3. BACKSTEPPING CONTROL DESIGN

Backstepping is a recursive procedure based on Lyapunov's stability theory, see Sepulchre et al. [1997]. Step-by-step, system states are chosen as virtual inputs to stabilise the corresponding subsystems. In this way a clf (Control Lyapunov Function) for the considered system is constructed and the control law is determined. Backstepping design can be applied to different classes of systems, e.g. systems in the so called strict feedback form, see Smaoui et al. [2004]. An overview of backstepping control is given by Krstić et al. [1995] or Khalil [1996].

3.1 Control of internal muscle pressure

The pneumatic subsystem represents a differential flat system with the internal muscle pressure as flat output, see Aschemann and Hofer [2006]. Hence, equation (6) can be solved for the mass flow as control input. As a result the mass flow $\dot{m}_{Mi}$ is given by the following inverse model depending on the flat output and its first time derivative

$$\begin{aligned} \dot{m}_{Mi} = &\frac{1}{k_{ui}(\Delta \ell_{Mi}, p_{Mi})} \cdot [\nu_{i1}(\dot{p}_{Mid}, e_{i1}) \\ &+ k_{pi}\left(\Delta \ell_{Mi}, \Delta \dot{\ell}_{Mi}, p_{Mi}\right) \cdot p_{Mi}] \ , \end{aligned} \tag{8}$$

with $\nu_{i1} = \dot{p}_{Mi}$ as the control input. For the pneumatic subsystem the dynamics of the tracking error $e_{i1} = p_{Mid} - p_{Mi}$, $i = \{1,2\}$, has to be stabilised

$$\dot{e}_{i1} = \dot{p}_{Mid} - \dot{p}_{Mi} \ , \tag{9}$$

where $\alpha_{i1} = \dot{p}_{Mi}$ serves as virtual input, which has to guarantee the convergence of the pressure error e_{i1} to zero via special feedback design. Therefore, a quadratic Lyapunov function is chosen

$$V(e_{i1}) = \frac{1}{2} \cdot e_{i1}^2 > 0 \ . \tag{10}$$

Its time derivative has to be negative definite

$$\dot{V}(e_{i1}) = e_{i1} \cdot \dot{e}_{i1} = e_{i1} \cdot \underbrace{(\dot{p}_{Mid} - \alpha_{i1})}_{\stackrel{!}{=} -a_{i1} \cdot e_{i1}} \ . \tag{11}$$

Accordingly, the bracket in (11) is set to $-a_{i1} \cdot e_{i1}$ with the positive parameter $a_{i1} > 0$, which can be used to specify the control dynamics. Solving for the virtual control input results in

$$\alpha_{i1} = \dot{p}_{Mid} + a_{i1} \cdot e_{i1} \ . \tag{12}$$

For the pneumatic subsystems no further steps are needed. The stabilizing control law is given by equation (12), whereas the control input $\nu_{i1} = \alpha_{i1}$ has to be inserted in the inverse dynamics (8).

3.2 Control of the carriage position

The mechanical system part also represents a differential flat system with the rocker angle φ and the mean pressure $p_M = (p_{Ml} + p_{Mr})/2$ as flat outputs, see Aschemann and Hofer [2006]. Subsequent differentiation of the first flat output until one of the control inputs appear leads to

$$y_1 = \varphi \ , \dot{y}_1 = \dot{\varphi} \ , \tag{13}$$

$$\begin{aligned} \ddot{y}_1 &= \frac{1}{J(\varphi)} [-k(\varphi, \dot{\varphi}) + \tau - \tau_U] \\ &= \ddot{\varphi}(\varphi, \dot{\varphi}, p_{Ml}, p_{Mr}, \tau_U) \ , \end{aligned} \tag{14}$$

whereas the second variable directly depends on the pressures as control inputs

$$y_2 = p_M = \frac{1}{2}\left(p_{Ml} + p_{Mr}\right) . \tag{15}$$

The inverse dynamics can be obtained by solving the equations (14) and (15) for the input variables p_{Ml} and p_{Mr}. Hence, the input vector $\mathbf{u}$, depending on the angle φ, the angular velocity $\dot{\varphi}$, the desired mean pressure p_{Md} and the control input $v_2 = \ddot{q}$ is given by

$$\mathbf{u} = \begin{bmatrix} u_l \\ u_r \end{bmatrix} = \begin{bmatrix} p_{Ml}\left(\varphi, \dot{\varphi}, p_{Md}, v_2\right) \\ p_{Mr}\left(\varphi, \dot{\varphi}, p_{Md}, v_2\right) \end{bmatrix} . \tag{16}$$

The first subsystem of the outer control loop to be stabilised results from the definition of the tracking error $e_1 = \varphi_d - \varphi$. The time derivative becomes

$$\dot{e}_1 = \dot{\varphi}_d - \dot{\varphi} . \tag{17}$$

Here the virtual control input is given by $\alpha_1 \approx \dot{\varphi}$. As before, a quadratic Lyapunov function $V_1(e_1) = 1/2 \cdot e_1^2$ is used to stabilise the error dynamics. The virtual control input can be obtained by making the time derivative of $V_1(e_1)$ negative definite

$$\dot{V}_1(e_1) = e_1 \cdot \dot{e}_1 = e_1 \cdot \underbrace{\left(\dot{\varphi}_d - \alpha_1\right)}_{\stackrel{!}{=} -c_1 \cdot e_1 - c_2 \cdot e_1^3} , \tag{18}$$

with the parameters $c_1 > 0$ and $c_2 > 0$. In this way α_1 becomes

$$\alpha_1 = \dot{\varphi}_d + c_1 \cdot e_1 + c_2 \cdot e_1^3 . \tag{19}$$

For the next design step, the error variable e_2 is introduced

$$e_2 = \alpha_1(\dot{\varphi}_d, e_1) - \dot{\varphi} = c_1 \cdot e_1 + c_2 \cdot e_1^3 + \underbrace{\dot{\varphi}_d - \dot{\varphi}}_{= \dot{e}_1} . \tag{20}$$

The corresponding error dynamics is given by

$$\dot{e}_2 = c_1 \cdot \dot{e}_1 + 3 \cdot c_2 \cdot e_1^2 \cdot \dot{e}_1 + \ddot{\varphi}_d - \ddot{\varphi} , \tag{21}$$

with the virtual input $\alpha_2 = \ddot{\varphi}$. Again a Lyapunov function

$$V_2(e_1, e_2) = V_1(e_1) + \frac{1}{2} \cdot e_2^2 \tag{22}$$

is used for stabilisation. The time derivative has to be made negative definite

$$\begin{aligned} \dot{V}_2(e_1, e_2) =& e_1 \cdot \dot{e}_1 + e_2 \cdot \dot{e}_2 \\ =& -c_1 \cdot e_1^2 - c_2 \cdot e_1^4 + e_2 \cdot \underbrace{\left(\ddot{\varphi}_d - \alpha_2 + g_1\left(e_1, e_2\right)\right)}_{\stackrel{!}{=} -c_3 \cdot e_2 - c_4 \cdot e_2^3} , \end{aligned} \tag{23}$$

with $c_3 > 0$ and $c_4 > 0$. By setting the bracket in (23) to $-c_3 \cdot e_2 - c_4 \cdot e_2^3$ and solving for the virtual input α_2, the feedback control law follows as

$$\alpha_2 = \ddot{\varphi}_d + g_2\left(e_1, e_2\right) . \tag{24}$$

The control input $\alpha_2 = v_2$ has to be inserted in the inverse dynamics (16). Finally, the dynamics of the closed loop can be determined by the design parameters c_1, c_2, c_3 and c_4.

3.3 Adaptive backstepping of the carriage position

To consider model uncertainties represented by the disturbance torque τ_U in the control strategy, the adaptive backstepping approach can be used (Kokotović [1992], Krstić et al. [1995]). Therefore, the Lyapunov function (22) can be extended as follows

$$V_2 = \frac{1}{2} \cdot e_1 + \frac{1}{2} \cdot e_2^2 + \frac{1}{2 \cdot \gamma}\left(\tau_U - \hat{\tau}_U\right)^2 . \tag{25}$$

Here, the estimated disturbance torque $\hat{\tau}_U$ and the parameter $\gamma > 0$ are introduced. The equation of motion (1) yields the angular acceleration

$$\begin{aligned} \ddot{\varphi} =& -\frac{1}{J(\varphi)}\tau_U + \frac{1}{J(\varphi)}\left(\tau - k\left(\varphi, \dot{\varphi}\right)\right) \\ =& -\frac{1}{J(\varphi)}\tau_U + \alpha_2 , \end{aligned} \tag{26}$$

with the virtual input α_2 as before. Considering (25) and (26), the time differentiation of V_2 leads to

$$\begin{aligned} \dot{V}_2 =& -c_1 \cdot e_1^2 - c_2 \cdot e_1^4 + e_2 \cdot \left(\ddot{\varphi}_d - \alpha_2 + g_1(e_1, e_2) + \frac{\tau_U}{J(\varphi)}\right) \\ & - \frac{1}{\gamma}\dot{\hat{\tau}}_U\left(\tau_U - \hat{\tau}_U\right) . \end{aligned} \tag{27}$$

By rewriting, the right-hand side can be stated as

$$\begin{aligned} \dot{V}_2 =& -c_1 \cdot e_1^2 - c_2 \cdot e_1^4 + e_2 \cdot \left(\ddot{\varphi}_d - \alpha_2 + g_1(e_1, e_2) + \frac{\hat{\tau}_U}{J(\varphi)}\right) \\ & + \underbrace{\left(\frac{e_2}{J(\varphi)} - \frac{\dot{\hat{\tau}}_U}{\gamma}\right)}_{\stackrel{!}{=} 0}\left(\tau_U - \hat{\tau}_U\right) . \end{aligned} \tag{28}$$

The time derivative $\dot{V}_2$ can be made negative definite by choosing the expression multiplying e_2 equal $-c_3 \cdot e_2 - c_4 \cdot e_2^3$, whereas the expression multiplying $\tau_U - \hat{\tau}_U$ should disappear. This leads to the virtual control input and the differential equation for the disturbance torque estimation

$$\alpha_2 = \ddot{\varphi} + g_2(e_1, e_2, \hat{\tau}_U) , \tag{29}$$

$$\dot{\hat{\tau}}_U = \frac{e_2 \cdot \gamma}{J(\varphi)} . \tag{30}$$

The parameter $\gamma > 0$ can be used to determine the dynamics of the disturbance torque estimation.

3.4 Reduced nonlinear disturbance observer

As alternative approach to adaptive backstepping, disturbance behaviour and tracking accuracy in view of model uncertainties can be significantly improved by introducing a compensating control action provided by a nonlinear reduced-order disturbance observer. The observer design is based on the equation of motion. The key idea for the observer design is to extend the state equation with an integrator as disturbance model

$$\dot{\mathbf{y}} = \mathbf{f}\left(\mathbf{y}, \tau_U, \mathbf{u}\right), \quad \dot{\tau}_U = 0 , \tag{31}$$

where $\mathbf{y} = [\varphi, \dot{\varphi}]^T$ denotes the measurable state vector. The estimated disturbance torque is obtained from

$$\hat{\tau}_U = \mathbf{h}^T \cdot \mathbf{y} + z , \tag{32}$$

with the chosen observer gain vector $\mathbf{h}^T = [\, h_1 \;\; h_1 \,]$. The state equation for z is given by

$$\dot{z} = \Phi\left(\mathbf{y}, \hat{\tau}_U, \mathbf{u}\right) . \tag{33}$$

The observer gain $\mathbf{h}$ and the nonlinear function Φ have to be chosen such that the steady-state observer error $e = \tau_U - \hat{\tau}_U$ converges to zero. Thus, the function Φ can be determined as follows

$$\dot{e} = 0 = \dot{\tau}_U - \mathbf{h}^T \cdot \mathbf{f}\left(\mathbf{y}, \tau_U, \mathbf{u}\right) - \Phi\left(\mathbf{y}, \tau_U - 0, \mathbf{u}\right) . \tag{34}$$

In view of $\dot{\tau}_U = 0$, equation (34) yields

$$\Phi\left(\mathbf{y}, \tau_U - 0, \mathbf{u}\right) = -\mathbf{h}^T \cdot \mathbf{f}\left(\mathbf{y}, \tau_U, \mathbf{u}\right) . \tag{35}$$

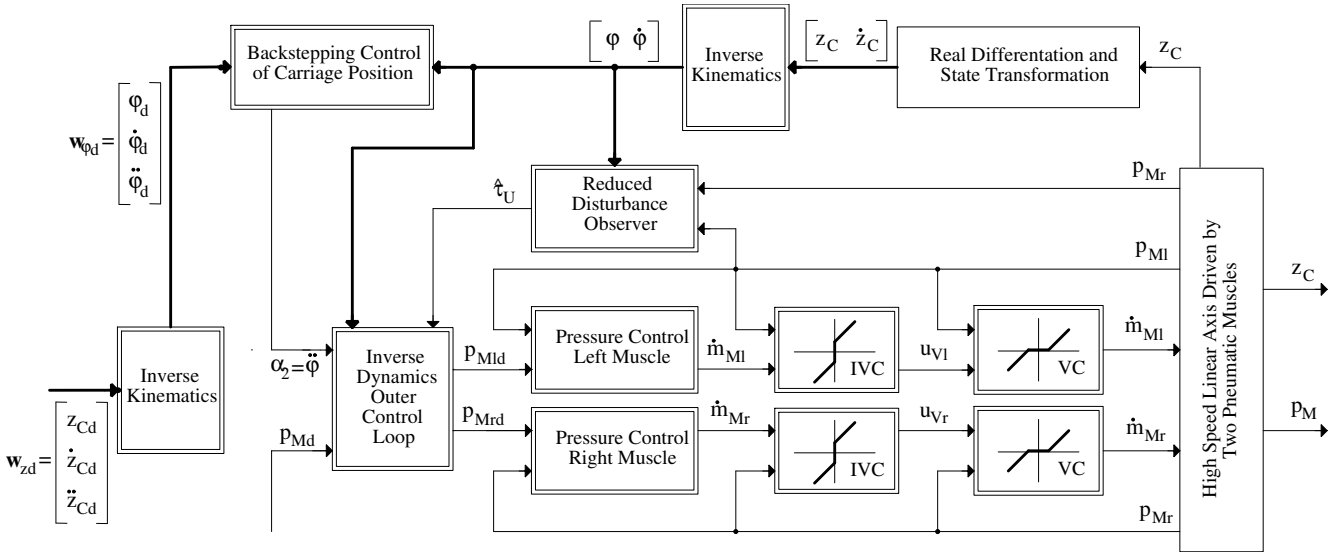

Fig. 5. Implementation of the backstepping control

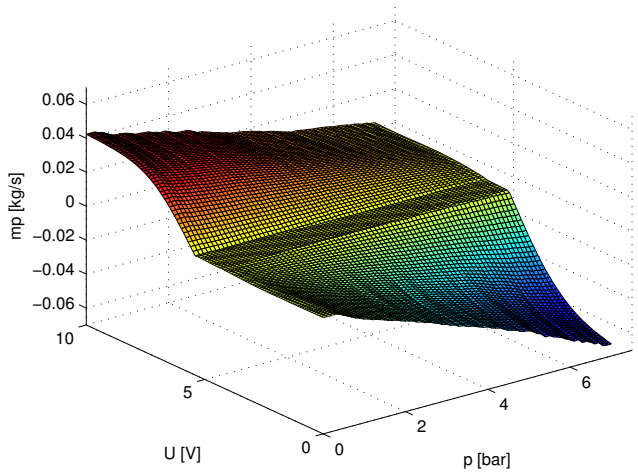

Fig. 6. Identified valve characteristic

The linearized error dynamics $\dot{e}$ have to be made asymptotically stable. Accordingly all eigenvalues of the Jacobian

$$\mathbf{J}_e = \frac{\partial \Phi(\mathbf{y}, \tau_U - e, \mathbf{u})}{\partial(\tau_U - e)} \tag{36}$$

must lie in the left complex half-plane. This can be achieved by proper choice of the observer gain h_1. The stability of the observer control system have been investigated by thorough simulations.

3.5 Compensation of the valve characteristic

The nonlinear valve characteristic (VC) is compensated by pre-multiplying with its inverse valve characteristic (IVC) in each input channel. The valve characteristic shown in fig. 6 has been identified by measurements. Here, the inverse valve characteristic depends both on the commanded mass flow and on the measured internal pressure and yields the appropriate input voltage u_{Vi} of the proportional valves as shown in fig. 5.

4. EXPERIMENTAL RESULTS

The described backstepping control scheme with the observer-based disturbance compensation has been implemented at the test rig of the the University of Rostock. It is equipped with two pneumatic muscles DMSP-40 from FESTO AG. The internal pressures of the muscles are measured by piezo-resistive pressure sensors, while the carriage position is determined by a linear incremental encoder with an accuracy of $10\mu m$. The control algorithm has been implemented on a dSpace real time system.

The desired trajectories for the carriage position, the internal pressures and their corresponding time derivatives are obtained from a trajectory planning module that provides synchronous time optimal trajectories. Here the desired $z-$position varies in an interval between -0.33 m and 0.33 m, see fig. 7. As can be seen, the maximum velocities are about $0.7m/s$. The mean pressure of the both muscles is kept constant on 4 bar during the whole experiment. For the compensation of the model uncertainties two strategies have been investigated: disturbance compensation by adaptive estimation and by disturbance observation yield similar results. The resulting tracking errors for the carriage position and the mean pressure obtained by adaptive backstepping control are depicted in the lower part of fig. 7. The maximum tracking error for the carriage position during the acceleration and deceleration intervals is approx. 1.5 mm, the maximum steady-state error is smaller than 80 μm. The tracking error of the mean pressure during the movements is below 0.1 bar, whereas the maximum steady-state pressure error is about 0.03 bar. In figure 8 the robustness of the controlled system regarding a changing mass of the carriage is demonstrated. An increase in the carriage mass $m_C = 18$ kg about 25 kg leads to a maximum position error of 3.5 mm, the steady state error is still smaller than 0.2 mm. The estimated disturbance torques from adaptive backstepping and nonlinear reduced disturbance observer are compared in fig. 9.

5. CONCLUSION

In this paper, a nonlinear cascaded trajectory control is presented for a high-speed linear axis driven by pneumatic muscles. To increase both the workspace and the maximum ve-

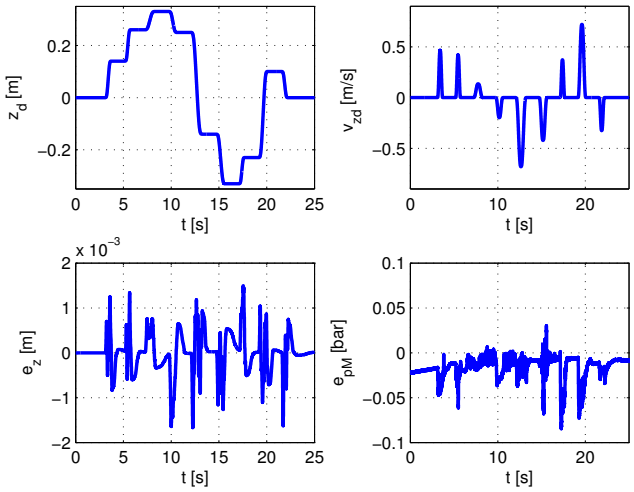

Fig. 7. Desired trajectories and according tracking errors for the carriage position and the mean pressure

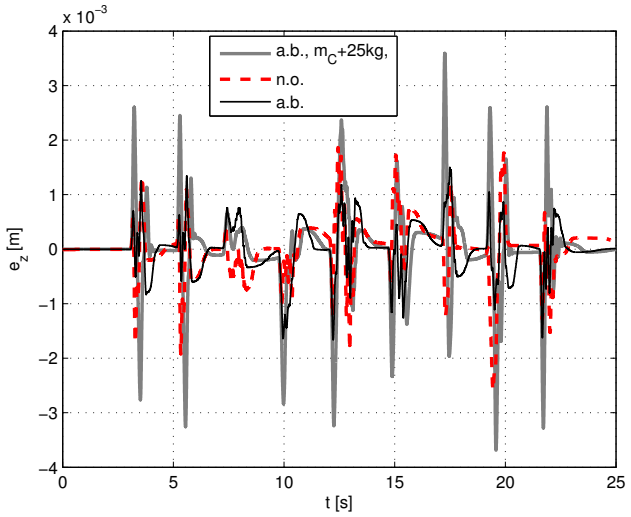

Fig. 8. Position error with adaptive backstepping (a.b.), nonlinear observer (n.o.) and changed mass of the carriage

locity, the muscles are linked to the carriage by a rocker in contrast to a directly actuated solution. The modelling of this mechatronic system leads to a system of nonlinear differential equations of fourth order. For the nonlinear characteristics of the pneumatic muscles polynomials serve as good approximations. As the nonlinear valve characteristic is linearised by means of a pre-multiplication with its approximated inverse characteristic, the mass flow represents the new control input. For both the inner and the outer control loop, backstepping controllers have been implemented. While the internal muscle pressures represent the controlled variables for the inner control loop, the rocker angle and the mean pressure are controlled in the decoupling outer loop. In order to compensate remaining uncertainties in the muscle force as well as the friction characteristic, either an adaptive estimation of the disturbance torque or a nonlinear disturbance observer can be employed in the control structure. Both disturbance compensation strategies show similar experimental results with good closed-loop performance. The maximum position errors are approx. 1.5 *mm* and the maximum pressure errors remain below 0.1 *bar*.

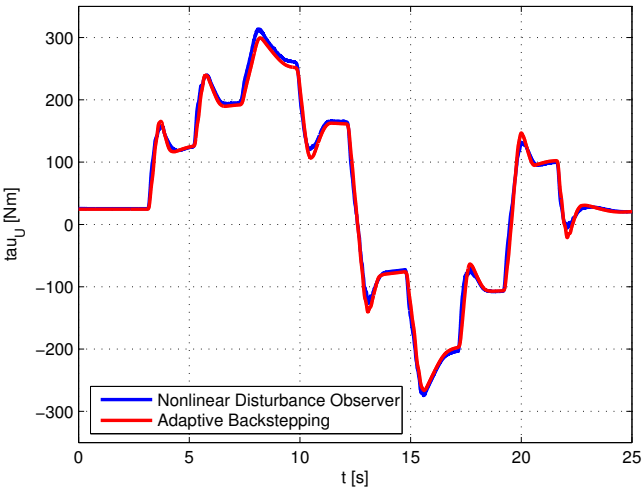

Fig. 9. Estimated disturbance torque

REFERENCES

H. Aschemann and E. P. Hofer. Nonlinear trajectory control of a high-speed linear axis driven by pneumatic muscle actuators. *Proceedings of the 32nd Annual Conference of the IEEE 2006, Paris, France*, pages 3857–3862, 2006.

H. Aschemann and D. Schindele. Nonlinear model predictive control of a linear axis based on pneumatic muscles. *Proceedings of ICINCO 2007, Angers, France*, pages 92–99, 2007.

H. Aschemann, D. Schindele, and E.P. Hofer. Nonlinear optimal control of a mechatronic system with pneumatic muscle actuators. *CD-Proceedings of MMAR 2006, Miedzyzdroje, Poland*, 2006.

P. Carbonell, Z.P. Jiang, and D.W. Repperger. Comperative study for three nonlinear control strategies for a pneumatic muscle actuator. *Proceedings of NOLCOS 2001, Saint-Petersburg, Russia*, pages 167–172, 2001.

M. Göttert. Bahnregelung servopneumatischer Antriebe. *Berichte aus der Steuerungs- und Regelungstechnik (in German), Shaker Verlag, Aachen*, 2004.

H. K. Khalil. *Nonlinear systems*. Prentice Hall, 1996.

P. V. Kokotović. Joy of feedback: Nonlinear and adaptive, (1991 bode prize lecture). Technical Report CCEC-92-0207, Center for Control Engineering and Computation. University of California at Santa Barbara, 1992. Published in Control Systems Magazine, 12:7-17, June 1992.

M. Krstić, I. Kanellakopoulos, and P. V. Kokotović. *Nonlinear and Adaptive Control Design*. John Wiley & Sons, 1995.

D. Schindele and H. Aschemann. Nonlinear model predictive control of a fast parallel robot actuated by pneumatic muscles. *CD-Proceedings of NOLCOS 2007, Pretoria, South Africa*, pages 206–211, 2007.

R. Sepulchre, M. Jankovic, and P. Kokotović. *Constructive Nonlinear Control*. Springer-Verlag, 1997.

M. Smaoui, X. Brun, and D. Thomasset. A robust multivariable control for an electropneumatic system using backstepping design. *Proceedings of NOLCOS 2004, Stuttgart, Germany*, pages 1193–1198, 2004.